

RESEARCH

Open Access



# Unveiling the potential of a functionalized pyrrole-based polymer for efficient cadmium ion removal from wastewater: synthesis, characterization, and performance evaluation

Marwa M. Sayed<sup>1</sup>, Islam S. Abd El-Hamid<sup>2,3</sup>, Haitham M. El-Bery<sup>4\*</sup>, Mostafa Farrag<sup>5</sup> and Kamal I. Aly<sup>2</sup>

## Abstract

Cadmium ion  $\text{Cd}^{2+}$  contamination is a major environmental issue caused by industry. Polyarylidene N-hexane pyrrole ( $\text{PAP}_h$ ) and crosslinked polyarylidene N-phenyl pyrrole ( $\text{PAP}_D$ ) were prepared from the previously synthesized polymer (polyarylidene ketone (PAK)) by using the advantage of repeating carbonyl groups at the 1,4 position and reacting it with hexylamine and P-phenylenediamine via the Paal–Knorr reaction. Various methods were used to characterize polymers, such as FT-IR spectroscopy, X-ray diffraction (XRD), thermogravimetry analysis (TGA), UV–visible spectroscopy, scanning electron microscope (SEM), zeta potential, and surface area measurements (BET), revealing successful fabrication, good thermostability, and well-defined microporous structures useful for  $\text{Cd}^{2+}$  adsorption. Optimal adsorption capacities of  $55.8 \text{ mg g}^{-1}$  for  $\text{PAP}_h$  and  $86.95 \text{ mg g}^{-1}$  for  $\text{PAP}_D$  indicate a significant enhancement in  $\text{Cd}^{2+}$  adsorption via their microporous structures,  $\text{Cd}^{2+}$  adsorption was also investigated in terms of contact time, initial concentration, and pH. A total input concentration of 30 ppm Cd ions, may yield an 84.3% removal rate for  $\text{PAP}_h$  and an 89.2% removal rate for  $\text{PAP}_D$ . The experimental results were well-fit by many models, including pseudo-second-order kinetics (PSO), Freundlich isotherms, intraparticle diffusion, and Langmuir. The varying adsorption performances of the two polymers studied, ( $\text{PAP}_h$ ) and ( $\text{PAP}_D$ ), were found to be derived from their respective chemical structures, which include various functional groups, according to studies conducted on  $\text{Cd}^{2+}$  in an aqueous solution.  $\text{Cd}^{2+}$  adsorption on polymers was considered physisorption;  $\pi$ -cation interactions and surface complexation played significant roles in adsorption. The PAP polymers may be considered promising substitutes and innovative adsorbents to remove  $\text{Cd}^{2+}$  ions from a water solution.

**Keywords** Cadmium, Polypyrrole, Adsorption mechanism, Kinetic, Isotherm

\*Correspondence:

Haitham M. El-Bery  
Haitham.El-Bery@aun.edu.eg

Full list of author information is available at the end of the article



© The Author(s) 2024. **Open Access** This article is licensed under a Creative Commons Attribution 4.0 International License, which permits use, sharing, adaptation, distribution and reproduction in any medium or format, as long as you give appropriate credit to the original author(s) and the source, provide a link to the Creative Commons licence, and indicate if changes were made. The images or other third party material in this article are included in the article's Creative Commons licence, unless indicated otherwise in a credit line to the material. If material is not included in the article's Creative Commons licence and your intended use is not permitted by statutory regulation or exceeds the permitted use, you will need to obtain permission directly from the copyright holder. To view a copy of this licence, visit <http://creativecommons.org/licenses/by/4.0/>.

## Introduction

Water's unique properties make it an essential and irreplaceable component for the survival and functioning of all living organisms. Therefore, any pollution of water resources would make it harder for people and other living things to maintain their health [1, 2]. Heavy metals are a significant threat to our water supply and a major contributor to the broad problem of environmental contamination caused by sources of pollution from industrial operations [3]. There is a growing trend of discharging these metals into environmental water, particularly in developing countries. One of the most significant environmental issues is pollution caused by these metals because of their toxicity and various negative consequences. Also, due to their solubility in water, they can be absorbed by organisms on Earth. [4, 5]. Large amounts of heavy metal ions may build in the human body once they reach the food chain. Intake of metal ions above the safe concentration can result in significant health problems [6]. One of the most dangerous heavy metal ions is cadmium ( $\text{Cd}^{2+}$ ) because it can cause considerable damage to the central nervous system and other essential organs in humans and animals when taken at more than safe levels [7]. Welding, electroplating, cadmium (Cd) and nickel (Ni) batteries, nuclear energy plants, paints, plastics, and fertilizers are all contributors to cadmium (Cd) pollution in both natural water bodies [8]. The rising global demand for most metals, the degradation of accessible ores, and severe environmental restrictions make it intriguing to identify effective and efficient ways for processing waste solutions containing metal ions, even at low concentrations. Most techniques for separating inorganic species from dissolved matrices, industrial fluids, and natural waters [8] involve liquid–liquid extraction, sorption, precipitation [9], coagulation-flocculation surface absorption, ions-exchanger [10], membrane filtration [11], and other two-phase distribution methods. Some issues might arise from using these strategies despite the fact that many of them have been created and used effectively. Certain complications may arise in relation to inter-phase transfer and heterogeneous reactions. Additional issues may develop if organic solvents or solid concentrates are selected for the following operations over aqueous solutions. When this happens, further steps such as reverse extraction, desorption, dissolving solid concentrates, etc., are required, which makes analysis more difficult and increases the risk of sample contamination from the added reagent [9, 10]. There has been a lot of research into and use of insoluble polymeric supports for recovering metals from weak solutions. Finding effective, low-tech solutions to the problem of heavy metal contamination in water samples is an area

worthy of study. Selecting an effective adsorbent material is crucial to purify water containing heavy metals. One example of an ion exchanger is the organic resins. Superior mechanical and chemical stability, as well as a high ion exchange capacity and rate, are the primary benefits. Many organic and inorganic materials [11–14] have been investigated for their potential application in wastewater purification. However, polymeric materials with donor atoms in their skeletal structures have been influential as adsorbents and represent a class of polymers that have found considerable use in environmental applications [15]. The ability to tailor the crosslinking degree and fixed ligand groups is a further benefit. It is possible to differentiate chelating polymers (polychelators) from polyelectrolytes. The former can create coordination bonds due to their functional groups, whereas the latter may be readily ionizable in water. The ligands found in polychelators that have been studied the most include amines, carboxylic acids, amides, alcohols, amino acids, pyridines, thioureas, iminos, and so on. Structures containing carboxylic acid, phosphoric acid, sulfonic acid, or ammonium groups are the most researched polyelectrolytes [16–19]. Copolymerization is a flexible method for synthesizing various polymers. It is feasible to enhance characteristics like water-solubility, metal ion binding capacity, and selectivity by carefully selecting both comonomers. These materials can coordinate with various metal ions due to their structural assembly [20–22].

Polypyrrole (PPy) has received much attention as a novel conducting polymer because of its high electric conductivity, excellent thermal stability, and beneficial environmental impact [23]. Using the Paal–Knorr reaction to add pyrrole rings to the backbone of functional alternating 1,4-polyketones has proven to be a promising way to produce functional polymers [24–28]. Under mild experimental conditions, the Paal–Knorr reaction can be performed without using catalysts and solvents [29–32]. The use of such a reaction to prepare polymeric amines is fascinating. Among the many uses for amine functional polymers are metal ions chelating agents [33].

This article's primary objective is to enhance the prepared alternating 1,4-polyarylidene ketone (PAK) performance in its capacity to adsorb ( $\text{Cd}^{2+}$ ) metal by increasing the number of chelating groups in the polymer structure. Thus, this research presents the synthesis and characteristics of two new functionalized amine polymers with pyrrole units along the backbone, derived from the (PAK) through its reaction with hexylamine and P-Phenylenediamine via Paal–Knorr reaction, and evaluates the (Cd) metal uptake behaviour of the newly prepared polymers in comparison to the original polymer.

## Experimental

### Chemicals and reagents

2,5-Hexane dione (97%), hexylamine (99%), and terephthaldehyde (98%) are from Alfa Aesar. Ethanol absolute EtOH (99.9%), methanol MeOH (99.9%), and p-phenylenediamine (99.5%) are from Sigma-Aldrich. Silica Gel (60–80) mesh pore size, hydrochloric acid HCl (35%), sodium hydroxide NaOH, acetone (99.9%), potassium hydroxide KOH, and cadmium chloride dihydrate  $\text{CdCl}_2 \cdot 2\text{H}_2\text{O}$ . All of the chemicals and organic solvents that are used are highly pure.

### Synthesis of polyarylidene ketone (PAK)

According to our previous work, the polymer (PAK) is synthesized by reacting terephthaldehyde with 2,5-hexane dione in an ethanolic solution [34].

### Synthesis of polyarylidene N-hexane pyrrole (PAPh)

In a flask (100 ml) fitted with a condenser and a magnetic stirrer, 1 g of prepared polymer (PAK) was first dispersed in about 50 ml absolute ethanol by stirring it for one hour. About 3 g (0.03 mol) of hexylamine was dissolved in 10 ml absolute ethanol and added to the previous solution until all were mixed. The reaction was performed under continuous stirring at ambient temperature for (24 h). Filtering, followed by water and ethanol washing and drying under decreased pressure at 80 °C for 24 h, separated the produced polymer with a dark orange colour from the original polymer.

### Synthesis of crosslinked polyarylidene N-phenyl pyrrole (PAPD)

In a flask (100 ml), about 1 g of PAK was dispersed and stirred in 50 ml absolute ethanol for one hour. The initial solution mixture was supplemented with 3.2 g of p-phenylenediamine (0.03 mol) that had been dissolved in 10 ml of absolute ethanol. The reaction was carried out at room temperature with constant stirring for 24 h. A brown-coloured polymer that had been produced was separated by filtering, washed with ethanol and water, and dried for 24 h under decreased pressure at 80 °C.

### Preparation of heavy metal Cd (II) solution

At room temperature, a stock solution of the heavy metal  $\text{Cd}^{2+}$  was made at a concentration of 20 ppm in distilled water [35].

### Measurements

Infrared spectra are measured with a Shimadzu 2110 PC Scanning Spectrophotometer. A Buck version 210 VGP Inc., East Norwalk, Connecticut, flame and graphite atomization methods (USA) is used as the atomic absorption apparatus for metal concentration detection.

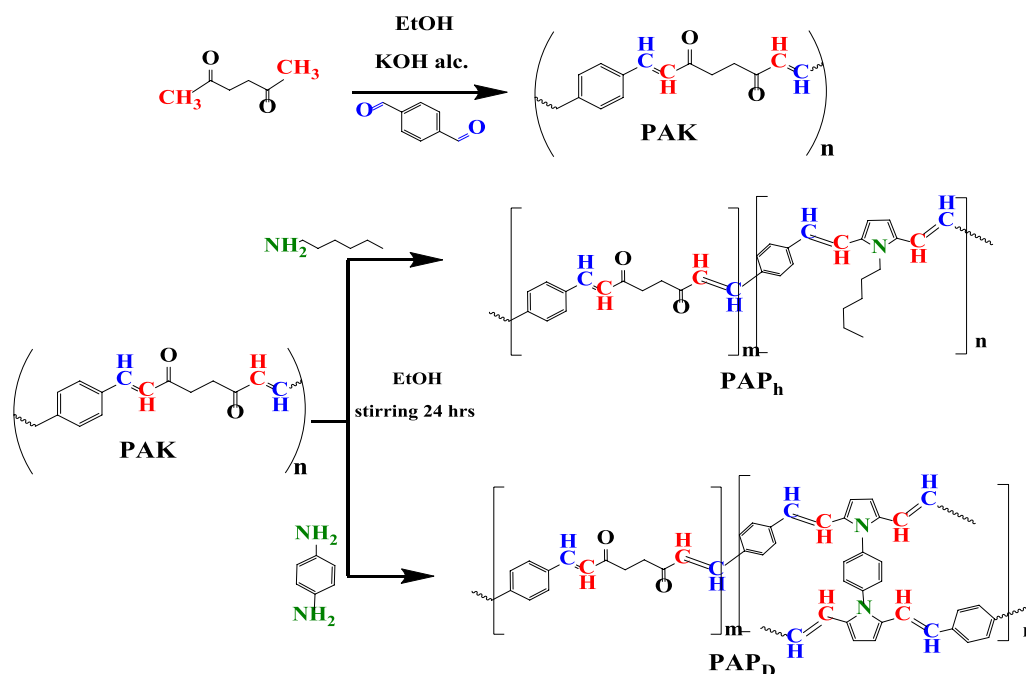
The Bruker D8 Advance, which is a copper tube that houses an X-ray device, is used to analyse polymer X-ray diffractograms. The X-ray source, which has a wavelength of 1.5406 nm, is powered by a generator that operates at 40 kV and 40 mA. The scanning range for the Coupled TwoTheta ( $2\theta$ ) is 5° to 60°, and the scanning rate is 0.02°/0.60 s. The samples are heated at 10 °C/min in an  $\text{N}_2$  atmosphere in a TA 2000 thermal analyzer and a Shimadzu DTG-60, respectively. Polymer morphology is studied using a scanning electron microscope (SEM), specifically a Joel- JSM-5400 LV. The Nova 3200 surface area instrument collects BET data in the  $\text{N}_2$  atmosphere. The UV–Vis spectra are measured with a Perkin-Elmer spectrophotometer using a 1-mm quartz cell.

## Results and discussion

Alternating 1,4-dicarbonyl groups along the polymer chain can be easily transformed into polythiophene, furan, or polypyrrole [36]. The “Paal–Knorr” synthesis yields functional groups retained along the main chain of N-substituted pyrrolic units with an aliphatic or aromatic substituent [37]. It is especially fascinating when used with molecules that alternate between polyketone and amine-substituted compounds. The Paal–Knorr reaction can be carried out without a catalyst or solvent and produces water as a byproduct under particular experimental circumstances. The Paal–Knorr mechanism is a unique example of a functionalization reaction in which both the level of functionalization and the aromatic density along the backbone can be modified at the same time.

The functionality of alternating polyketone emphasizes its unique characteristics compared to other functional polymers, such as polyolefins, polystyrene, and acrylates [38]. The increased backbone aromaticity may also have further applications, particularly in the hydrophobic interactions needed to disperse dyes, which hardens the polymer backbone. A quick, simple, and inexpensive Paal–Knorr reaction binds the primary amines hexylamine and p-phenylene to the previously synthesized 1,4-polyketone (PAK) core, yielding N-substituted pyrroles (Scheme 1). The amine solution is added after the polymer has been thoroughly mixed in an ethanolic solution, and the mixture stays for 24 h with continuous stirring at room temperature. The resultant improved polymers are examined for pyrrole units in the modified polymers using several studies.

The structure of polypyrrole PPy in the literature is consistent with the FT-IR analysis data in Fig. 1, which also demonstrates the distinction between the resultant polymers (PAP<sub>h</sub>, PAP<sub>D</sub>, and PAK). [39–43]. In contrast to the PAK spectrum, the C–N pyrrole stretching bands are visible in the polyamine spectrum at 1172  $\text{cm}^{-1}$  and 1379  $\text{cm}^{-1}$  for PAP<sub>h</sub> and 1167  $\text{cm}^{-1}$  and 1365  $\text{cm}^{-1}$  for



**Scheme 1** Synthesis of PAK, PAP<sub>h</sub>, and PAP<sub>D</sub>

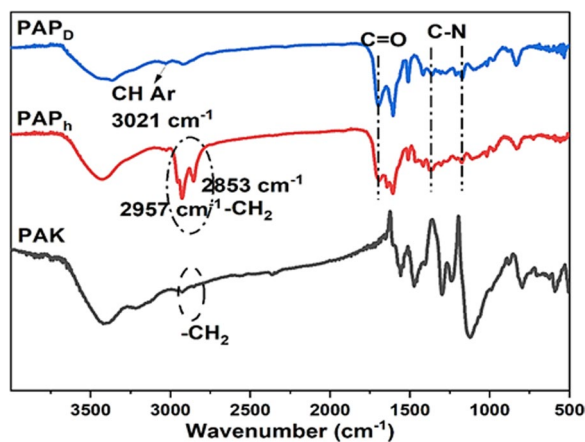


**Fig. 1** FT-IR spectra of PAK, PAP<sub>h</sub>, and PAP<sub>D</sub>

PAP<sub>D</sub>. The stretching vibration of the aliphatic hexyl chain appears more clearly in the PAP<sub>h</sub> spectrum than in the PAK or PAP<sub>D</sub> spectra. The spectrum of PAP<sub>h</sub> demonstrates that the stretching vibration of C=C pyrrole ring bands at 1510 cm<sup>-1</sup>, aromatic stretching vibrations at 1610 cm<sup>-1</sup>, and peak at 1422 cm<sup>-1</sup> is due to the bending vibration of the C-H aliphatic bond [40, 44]. The stretching vibration of C=C pyrrole rings is visible in the spectrum of PAP<sub>D</sub> at 1511 cm<sup>-1</sup>, and the stretching vibration of aromatic bonds is at 1607 cm<sup>-1</sup>. The C-H aliphatic bond's bending vibration appears at 1414 cm<sup>-1</sup> [39, 40, 43].

Additionally, the PAP<sub>D</sub> spectrum shows a lower stretching vibration of the aliphatic chain than the PAK or PAP<sub>h</sub> spectra, indicating that the polymer backbone is more aromatic than PAK. C=O stretching in the FT-IR spectra of PAP<sub>h</sub> and PAP<sub>D</sub> is seen at 1691 cm<sup>-1</sup> and 1699 cm<sup>-1</sup>, respectively. That peak is due to the conjugation of a non-reactant carbonyl group along the chain. The stretching vibration peak of C-O showed at 1294 cm<sup>-1</sup> in the spectrum of PAK, indicating the presence of the keto-enol form in the chains [45]. As a regioselective reaction, the Paal-Knorr reaction is inhibited by steric hindrance, making primary amine groups attached to secondary or tertiary carbons less reactive than those connected to primary carbons [36]. In the case of PAP<sub>h</sub>, the hexyl chain has an electron-donating action that would increase the electron density on the N and make cyclization easier. According to PAP<sub>D</sub>, the phenyl ring's terminal group has an amino group, which promotes cyclization by acting as an electron donor; the reaction proceeds at room temperature [46].

According to the XRD data in Fig. 2a, the modified polymers have X-ray graphs extending to greater angles around 19.9–20.1° compared to the original PAK [47], which has a peak at 13°. These peaks demonstrate that the pyrrole rings are formed in the polymer chain at this location. It can be deduced from the patterns that the amorphous areas in the polymer backbone make the produced polymers less crystalline than PAK (56.7% crystallinity), as PAP<sub>h</sub> has 42.8% crystallinity and PAP<sub>D</sub>

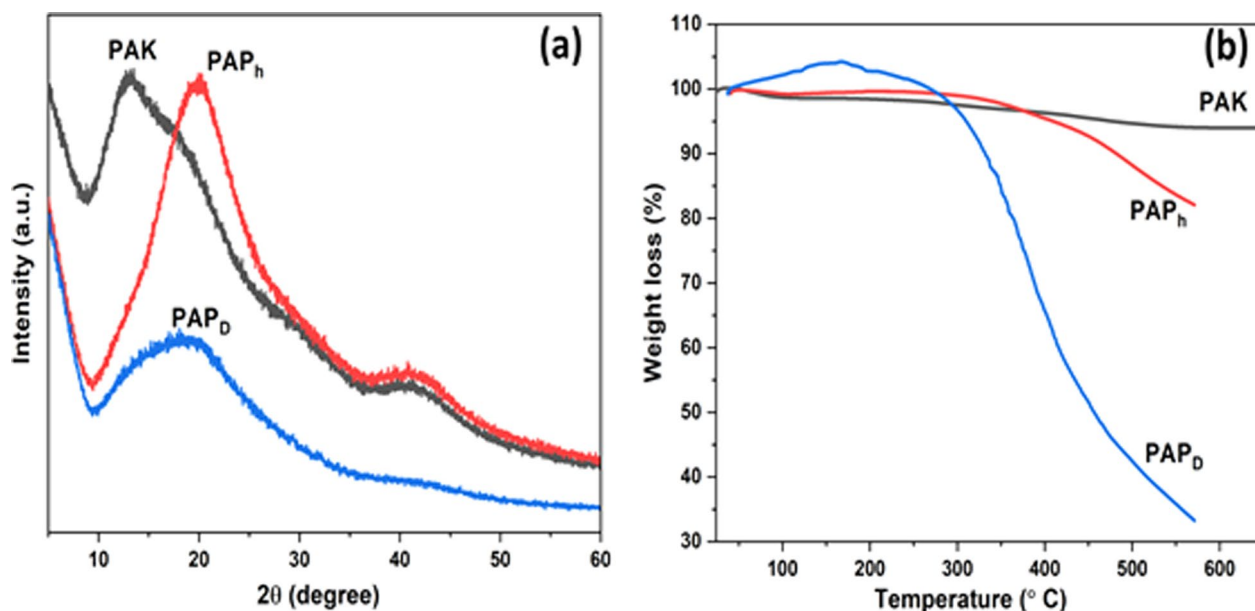


**Fig. 2** a XRD graphs, b TGA curves of PAK, PAP<sub>h</sub>, and PAP<sub>D</sub>

**Table 1** Temperature (°C) for various decomposition levels in N<sub>2</sub> at a heating rate of 10 °C/min

Polymer	4% wt. loss	5% wt. loss	10% wt. loss	Char yield (%) at 600 °C
PAK	421	478	>600	94
PAP <sub>h</sub>	388	410	482	82
PAP <sub>D</sub>	305	310	332	33

has 39.3% crystallinity. In PAP<sub>h</sub>, the aliphatic chain that is present in hexyl amine provides some flexibility to the mobility of the chains, which ultimately results in less space or distance between polymer chain molecules. The introduction of crosslinking through p-phenylene molecules reduces PAP<sub>D</sub>'s flexibility and mobility, affecting the physical characteristics of polymeric materials and increasing the proportion of amorphous areas in the polymer.

Figure 2b shows the results of a thermogravimetric analysis (TGA) that demonstrates the thermal stability of the prepared polymers; Table 1 provides data on the initial degradation temperature and char yield at 600 °C of the prepared polymers. According to the results, the synthesized polymers are stable, with the initial degradations occurring at higher temperatures (4% weight loss for PAK 421 °C, 388 °C for PAP<sub>h</sub>, and 305 °C for PAP<sub>D</sub>). The PAK polymer is more stable and yields higher char than the modified polymers. PAP<sub>D</sub> shows more rapid degradation than the other polymers. After reaching 302 °C, a rapid

decrease in mass continues, which may be attributable to the systemic thermal breakdown of the polymer chains that contain pyrrole rings. These findings demonstrate the formation of pyrrole rings in the polymer chains with a great percentage. Also, they are carbonized to create graphitic structures and cannot entirely decompose completely in a nitrogen atmosphere [48]. X-ray results suggest that the crosslinked polymer PAP<sub>D</sub> has an amorphous structure and, hence amorphously arrangement of chains containing pyrrole rings, which may explain why the degradation of the produced crosslinked polyamine is accompanied by a faster weight loss than that of PAP<sub>h</sub> and PAK [43]. The thermal conductivity and stability increase with increasing crystallinity; polymers show significant anisotropy in their thermally conductive qualities since heat transfers more readily along the direction of the polymer chains rather than perpendicular to them and hence retard the heat transfer between the chains [49]. Since PAK has the finest packing of the chains and has a more significant crystallinity percent, it is more thermally stable than the other polymers.

As shown in Fig. 3, microstructural analyses of produced polymers provide further evidence that the chain reaction has succeeded. Compared to PAK, PAP<sub>h</sub> has a more aggregated structure; its particles are more uniform in size and shape, prefer to aggregate, and take on a spherical shape. In contrast, in PAP<sub>D</sub>, the spherical particles aggregate into stacked blocks with unequal shapes and a rough surface by further smoothing and linking the particles [50, 51]. PAP<sub>D</sub>'s structure results from crosslinking in the structure and distribution of pyrrole

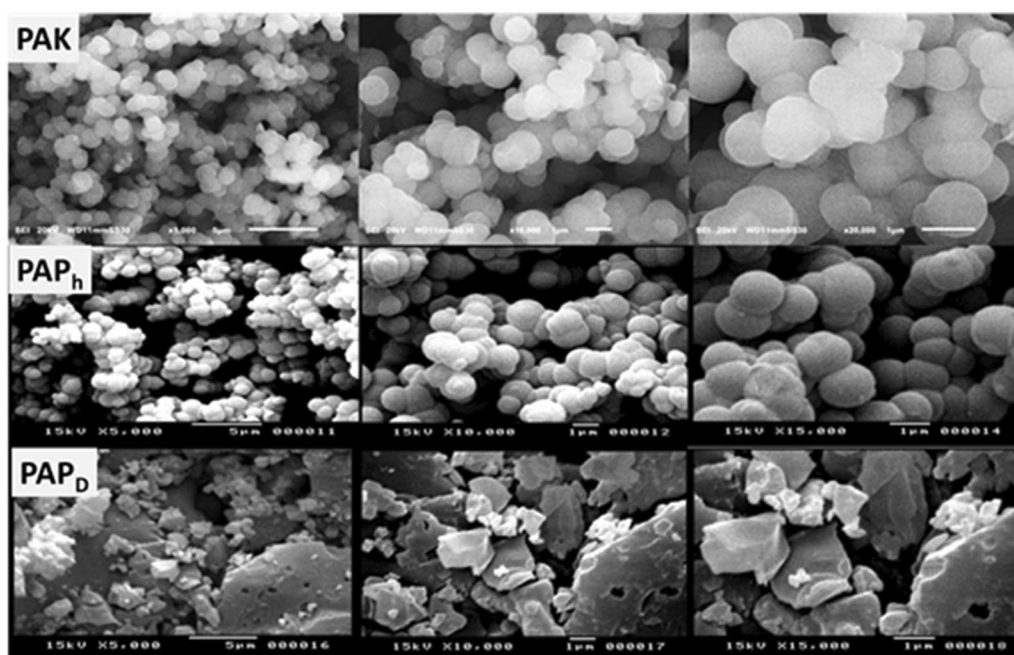


**Fig. 3** SEM images at different magnifications of PAK, PAP<sub>h</sub>, and PAP<sub>D</sub>

rings between chains in its three-dimensional structure, resulting in an amorphous structure as opposed to PAP<sub>h</sub>'s structure, which lacks this crosslinking. The results showed that pyrrole rings were synthesized along PAK chains [51].

The development of pyrrole rings throughout the PAK chain was investigated using UV–visible spectroscopy, with absorbance recorded for a partially soluble solution of PAP<sub>h</sub>, PAP<sub>D</sub> (1 mg in 10 ml DMF). The polymers created by reacting PAK with various amines showed lower absorbance intensity in their spectra of absorbed light. Based on what we see in Fig. 4, like the original polymer PAK, PAP<sub>h</sub> has an absorbance peak at  $\lambda_{\max}$  269 nm and a shoulder peak at a longer wavelength at  $\lambda_{\max}$  276 nm. However, the peak at 269 nm in PAK polymer is also present in the PAP<sub>D</sub> spectrum with a noticeable broadening that does not exist in the other spectra [39]. As the data show, these results may be due to the increased chain conjugation, causing the additional peak and broadening to appear at a longer wavelength. One approach to learning about the structure and effects of the synthesized polymers due to interactions with other molecules is to measure their optical energy gap. It is influenced by conjugation in polymer molecules or semiconducting materials and measures the minimal energy necessary for electron excitation from the valence band to the conduction band. One may use Tauc's equation to determine the optical energy gap and optical transition from the absorption spectra [52]. Even though the optical energy

gap has been measured, Tauc's equations can be used directly to determine its transition. The absorbance maximum is increased by the presence of pure enone groups in the PAK transition, as opposed to double bonds with C–N bonds [53]. From Tauc's equation, the energy band gaps are calculated to notice the difference between the prepared polymers, compared to PAK (Eg 3.83 eV), the band gaps of the resultant polymers (PAP<sub>h</sub> 4.1 eV, PAP<sub>D</sub> 4.33 eV) are increased [54]. This increase in band gap is attributed to the formation of pyrrole rings between the aromatic rings of PAK, which increases the number of defect locations present among PAK's HOMO and LUMO states [47].

Solid-state PL spectra of polymers exhibit an emission peak at 377 nm with an excitation wavelength  $\lambda_{\text{exc}}$  of 280 nm; the polymers emit blue light. The Commission International de L'Eclairage (CIE) coordinate values for polymers are as follows: PAK (0.113, 0.297) (blue-green colour), PAP<sub>h</sub> (0.120, 0.248), and PAP<sub>D</sub> (0.124, 0.223) (greenish blue) the blue colour emission is increased gradually, as it known that the increase in the blue degree has occurred when the (y) coordinate is decreased [55, 56]. The  $\pi$ – $\pi$  interaction between polymer molecules is largely responsible for the colour produced; the crosslinking of PAP<sub>D</sub> makes this interaction particularly strong [57]. The colour change indicates pyrrole ring development along PAK chains.

Figure 5 and Table 2 provide N<sub>2</sub> adsorption–desorption isotherms and pore size distribution curves for

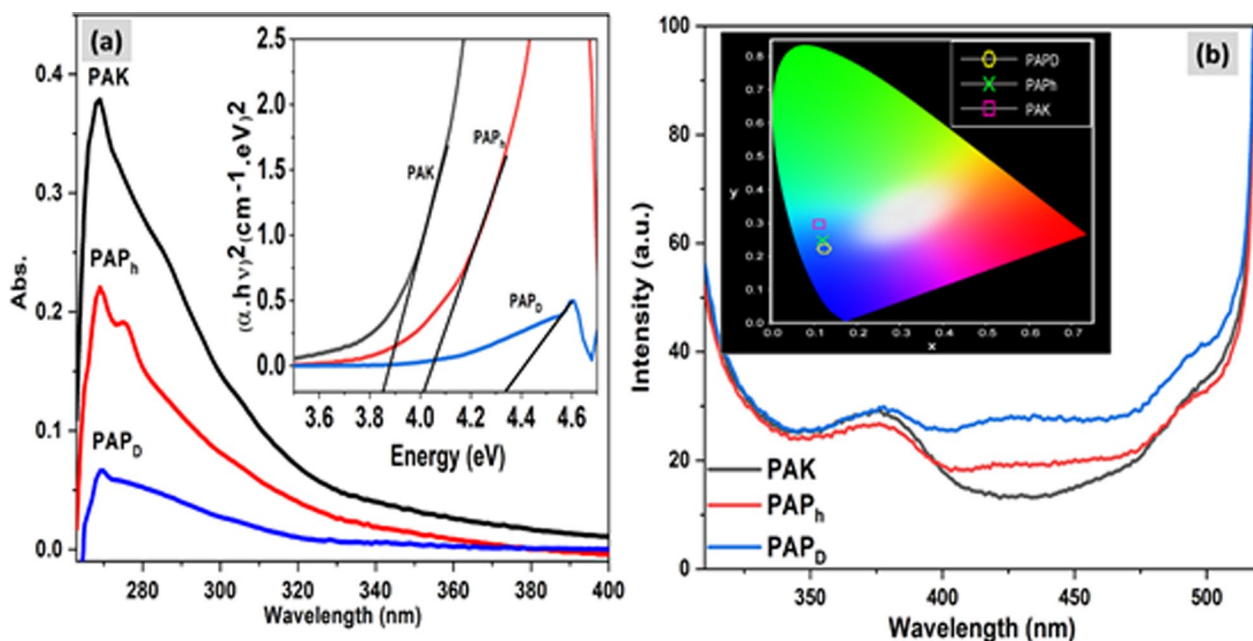


**Fig. 4** a UV–visible spectra, the inset graphs show energy band gap. b Emission spectra at  $\lambda_{exc}$  280 nm, and the inset photo shows the CIE diagram of PAK, PAP<sub>h</sub> and PAP<sub>D</sub>

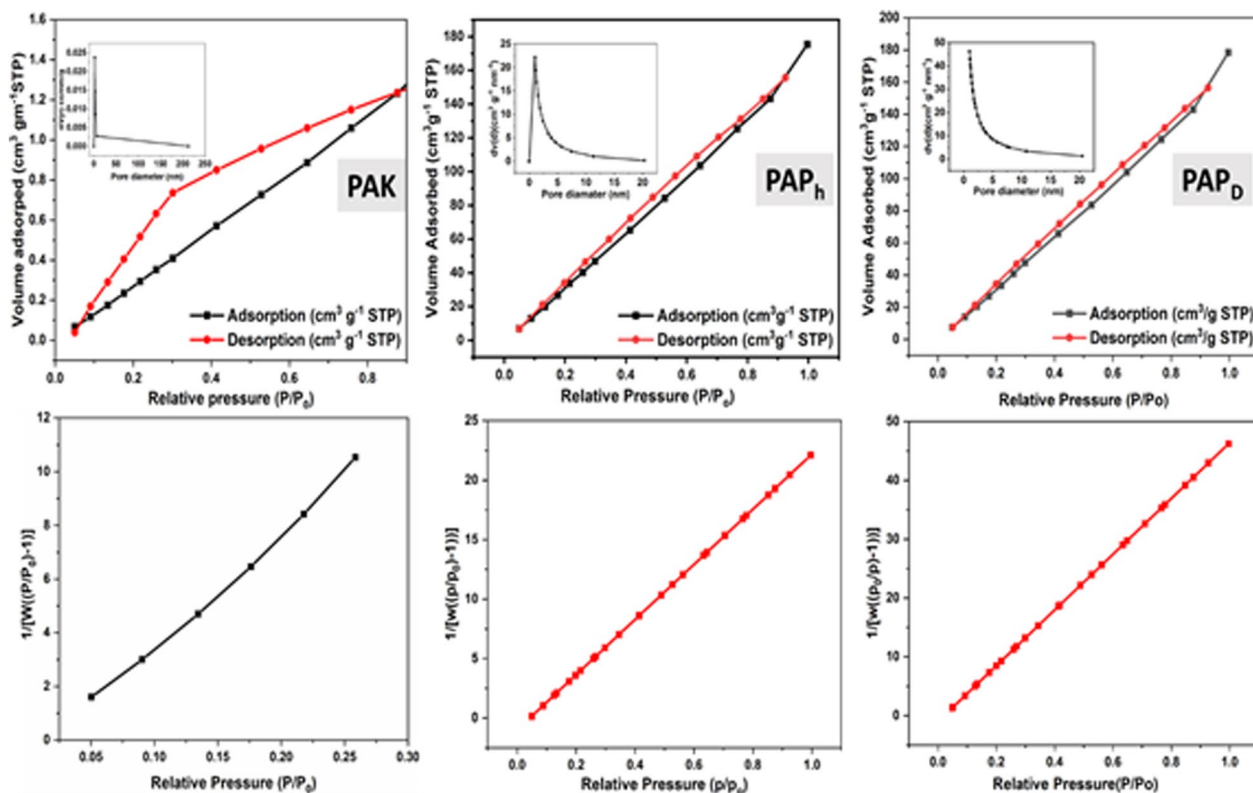


**Fig. 5** BET nitrogen adsorption isotherms (inset plots), pore size distribution, and BET surface area of PAK, PAP<sub>h</sub>, and PAP<sub>D</sub>

**Table 2** The surface area data for the prepared polymers

	PAK	PAP <sub>h</sub>	PAP <sub>D</sub>
N <sub>2</sub> adsorption cm <sup>3</sup> gm <sup>-1</sup> STP	1.46679	1.78388	1.7539
APS (avg. pore size) nm	1.7911	1.855	1.7
BET(surface area) m <sup>2</sup> gm <sup>-1</sup>	76.72	141.3	74
Pore volume cc gm <sup>-1</sup>	0.058	0.1129	0.055
BJH (pore radius) nm	1.915	1.1913	1.912
TPV (total pore volume) cc gm <sup>-1</sup>	0.0687	0.1311	0.063

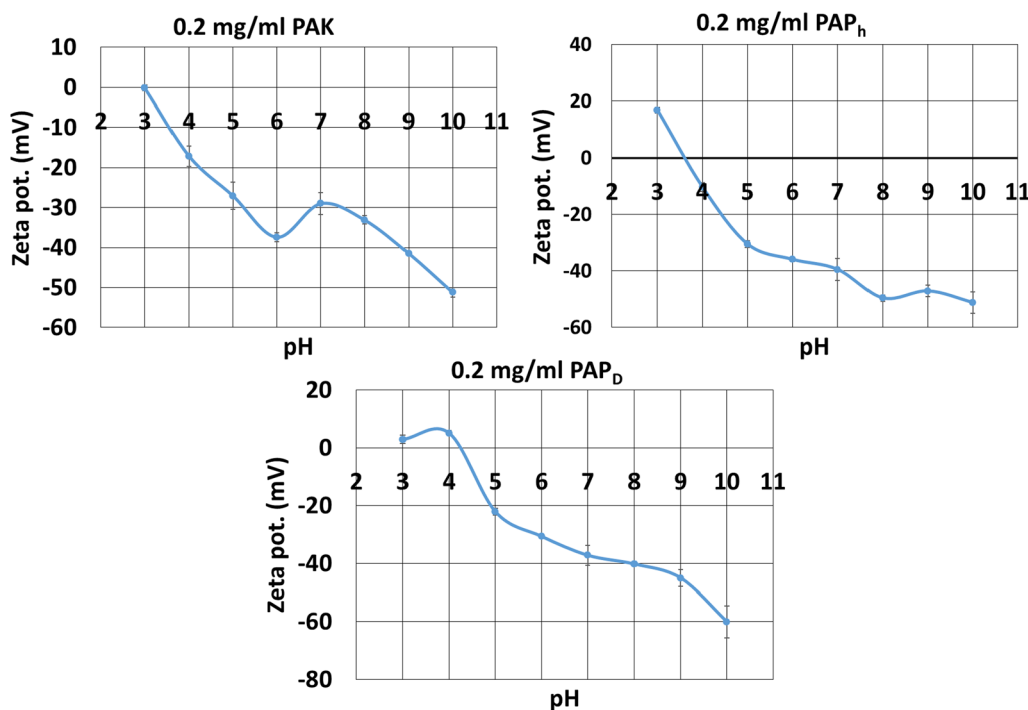
PAK, PAP<sub>h</sub>, and PAP<sub>D</sub>, respectively. All the curves show sorption patterns, indicating the microporous structure's presence. Compared to PAK's surface area of 76.72 m<sup>2</sup> g<sup>-1</sup>, the results show that PAP<sub>h</sub>'s specific surface area increases to 141.3 m<sup>2</sup> g<sup>-1</sup>, and that of PAP<sub>D</sub> decreases to 74 m<sup>2</sup> g<sup>-1</sup>. The polymers' pore sizes also altered, increased in PAP<sub>h</sub> at 1.83 nm and shrank in PAP<sub>D</sub> at 1.7 nm compared to PAK at 1.7911 nm. The results suggest that the polymer has pores that are near to being microporous. PAP<sub>h</sub>'s improved specific surface area to PAP<sub>D</sub> may be related to the presence of an aliphatic hexyl chain in the nitrogen of the produced pyrrole rings, which prevents the aggregation of the pyrrole rings and polymer chains [58–60].

In contrast to p-phenylene, the specific surface area decreases because pyrrole rings tend to aggregate. The overall area may be proportionate to the coiled portions

of chains that keep them from gathering and creating permeable parts when the chains are rigid and unable to compress and versatile chain integration. It would be difficult for the probe to contact the contact surface because neighbouring chains would rub against one another due to the packing. The phenyl ring connecting the pyrrole rings between chains and moieties reduces the surface area. Under these circumstances, the phenyl rings effectively fill a concave space on the molecule's surface. Simultaneously, the surface area rises because the hexyl chain extends far from the surface [61, 62].

Any particles on the surface of a macromolecule or substance have a property called zeta potential, which is a physical feature. Film and coating production may be optimized, and surface interactions predicted with this approach. Particles in suspension with a negative zeta potential tend to become even more negatively charged when additional alkali is added to the mixture. Sometimes, the acid added to this solution will neutralize the charge. If the acid is added in large enough quantities, the ions may be selectively adsorbed, leading to a buildup of positive charge. For this reason, the slope of a zeta potential vs. pH curve will be positive in acidic conditions and negative in basic ones [63].

Figure 6 depicts typical zeta potential curves of polymers. The results showed that PAP<sub>h</sub> adsorbed ions more strongly than PAP<sub>D</sub> and PAK at low pH, suggesting that PAP<sub>h</sub> possesses a considerable positive zeta potential

**Fig. 6** Plots of zeta potential vs. pH showing the position of the isoelectric point of PAK, PAP<sub>h</sub>, and PAP<sub>D</sub>



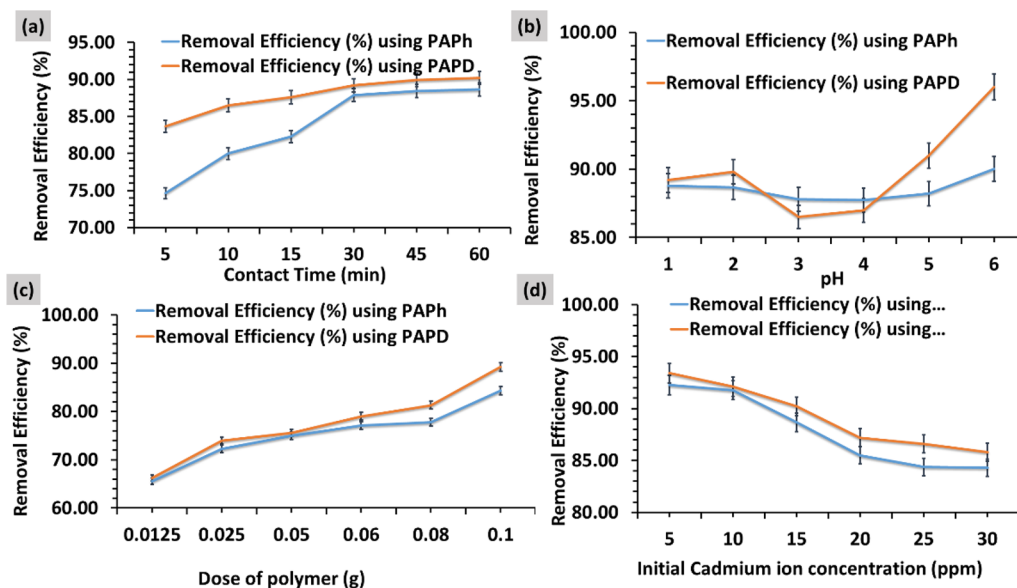


**Fig. 7** Study the effect of **a** contact time (pH=7, polymer dose=0.1 g, initial Cd<sup>2+</sup> concentration=20 ppm, T=293.15 K); **b** pH (polymer dose=0.1 g, initial Cd<sup>2+</sup> concentration=20 ppm, contact time=60 min, T=293.15 K); **c** polymer dose (initial Cd<sup>2+</sup> concentration=20 ppm, T=293.15 K, contact time=60 min, pH=7); and **d** initial Cd<sup>2+</sup> concentration (pH=7, polymer dose=0.1 g, contact time=60 min, T=293.15 K) on Cd<sup>2+</sup> adsorption efficiency of PAP<sub>h</sub> and PAP<sub>D</sub>

at low pH. Isoelectric points, where molecules do not carry a net electrical charge on average, occur at about pH 3, 3.6, and 4.2 for PAK, PAP<sub>h</sub>, and PAP<sub>D</sub>, respectively. In contrast to PAP<sub>D</sub> and PAP<sub>h</sub>, which have pyrrole rings in their chain and other phenyl rings in PAP<sub>D</sub> that increase the stacking effect and electrostatic attraction, PAK has more electron charge (carbonyl groups) on its surface, needs to be neutralized, and requires a strong acid medium. Therefore, the ion adsorption responses of PAP<sub>h</sub> and PAP<sub>D</sub> are distinct, as is the PAK polymer structure [64, 65].

### Studying the adsorption of Cd<sup>2+</sup> from wastewater through the produced polymers

#### Adsorption study

**Determination of optimum pH, polymer dose, and initial ion concentration:** The effectiveness of the produced polymers in removing Cd<sup>2+</sup> ions from an aqueous solution was investigated through a batch adsorption method. Experiments on adsorption in batches were performed at 700 rpm using a magnetic stirrer, and the pH of the Cd<sup>2+</sup> solution was monitored using a pH meter. CdCl<sub>2</sub>·2H<sub>2</sub>O was dissolved in purified water to produce Cd<sup>2+</sup> ion-loaded solutions. Then, at room temperature and for one hour, multiple adsorption tests were conducted to determine the optimal pH, polymer doses, initial cadmium concentration, and contact time.

The adsorption study was investigated by adding optimal amounts of PAP<sub>h</sub> and PAP<sub>D</sub> in powder form to the

flasks containing Cd<sup>2+</sup> feed solutions (200 ml each) ranging in concentration from 5 to 30 ppm at the optimal pH. The polymer samples were left in the cadmium solution and stirred until a stable state was reached. Adsorbed cadmium levels on the polymers were determined using the mass balance Eq. (1):

$$Q_e = \frac{(C_0 - C_e)V}{W} \quad (1)$$

In this equation,  $V$  represents the volume of the solution,  $W$  represents the weight of PAP<sub>h</sub> and PAP<sub>D</sub>,  $C_0$  is the starting concentration of cadmium ions in the solution, and  $C_e$  is the equilibrium concentration. For approximately 1 h, 5 ml aliquots of the solution were collected, and the remaining concentration of Cd<sup>2+</sup> ions was determined by atomic absorption analysis. The amount of Cd<sup>2+</sup> adsorbed by polymer molecules during a certain exposure period,  $q_t$  (mg g<sup>-1</sup>), was calculated as follows [66]:

$$q_t = \frac{(C_i - C_t)V}{m} \quad (2)$$

The notation referred as:  $C_i$ =initial Cd<sup>2+</sup> concentration (mg l<sup>-1</sup>),  $C_t$ =concentration at time  $t$  (mg l<sup>-1</sup>),  $V$ =volume of solution (L), and  $m$ =mass of the polymer sample (g).

Figure 7a-d displays adsorption studies with varying contact times, pH values, polymer doses, and initial Cd<sup>2+</sup> concentration. The influence of contact time between

polymers and metal ion solution at a pH of the solution was investigated by measuring the absorption of adsorbate ( $\text{Cd}^{2+}$ ) per mass of adsorbent across contact durations  $t$  ( $q_t$ ) ranging from 5 min to 1 h. Figure 7a shows that the probability of polymer removal rises with the increase in the contact time between the polymer and the solution. Within 60 min, all the polymers had attained equilibrium regarding their adsorption ability for cadmium ions. After 30 min, the capacity of both polymers is quite comparable and gradually rises until they approach equilibrium; however, in the first 30 min, the adsorption capacity of  $\text{PAP}_D$  is larger than that achieved by the  $\text{PAP}_h$  by roughly 10%.  $\text{PAP}_D$  showed around 90.2% effectiveness in adsorbing metal ions at equilibrium, making it the most effective adsorbent. The increased performance in  $\text{PAP}_D$  adsorption results from the larger available surface area.

The pH of the solution may significantly impact the adsorption characteristics of metal ions [14]. This study analysed the effects of pH on cadmium removal efficiency from acidic to basic solutions. The HCl and NaOH were used to make the acidic and basic solutions. At ambient temperature, a 0.1 gm sample of the polymers was submerged for 60 min in a 15 ppm cadmium solution. Figure 7b shows how the pH level affects the polymers' ability to remove metal ions; adsorption effectiveness is lower at acidic pH levels (3 and 4) and begins to rise from pH 5 and after for  $\text{PAP}_D$ , while the removal efficiency for  $\text{PAP}_h$  is almost the same at acidic pH (from 1 to 5) and begins to increase after pH 5. Saturation was obtained at a pH of 7.0 for all polymers tested regarding cadmium ion elimination. Apparent patterns and unfavourable adsorption of cadmium at low pH can be explained because of the repulsive electrostatic interaction between the positively charged cadmium ions and the protonated surface sites or may be due to the hydronium ions ( $\text{H}_3\text{O}^+$ ) competing with  $\text{Cd}^{2+}$  ions for adsorption sites at more acidic pHs, which limits the availability of cadmium ions. As the pH rises, the surface becomes more reactive to deprotonation, which favours the attachment of metal ions. Also, we can observe from the chart that the efficiency of  $\text{PAP}_D$  is higher than that of  $\text{PAP}_h$  at all pH levels except for pH levels (after 2.5 to 4). The results agree with zeta measurements of increased stacking in  $\text{PAP}_D$ , leading to decreased electrostatic attraction and increased zeta potential in the positive range before reaching the neutralization point in that range of pH values. Adsorption of  $\text{Cd}^{2+}$  ions occurs by physical adsorption between counter-charged particles; this is facilitated by the material's charge, which increases when the pH rises above 5. All the adsorption studies were performed at a pH of 7, where the removal effectiveness for  $\text{PAP}_h$  is about 90% and around 97% for  $\text{PAP}_D$ , as in solutions with a pH

greater than 7, cadmium ions precipitate as cadmium hydroxides [67].

For detecting the optimal  $\text{PAP}_h$  and  $\text{PAP}_D$  doses, adsorption studies were performed at neutral pH and dosages ranging from 0.0125 to 0.1 g/ 200 ml. According to the results shown in Fig. 7c, a concentration of 0.1 g/ 200 ml is sufficient to achieve about 84.3% Cd ion removal for  $\text{PAP}_h$  and 89.2% for  $\text{PAP}_D$  when the total feed concentration of Cd ion is 30 ppm. Therefore, the best initial cadmium concentration that gives high efficiency of removal can be determined by using these adsorbents doses and pH 7; the chart demonstrates that 92.3 and 93.4% of Cd ion can be removed at an initial concentration of 5 ppm with doses of 0.1 g/ 200 ml  $\text{PAP}_h$  and  $\text{PAP}_D$ , respectively (Fig. 7d).

#### Adsorption isotherm

The most popular models, the Freundlich and Langmuir isotherms [19], were utilized to fit the equilibrium data in this investigation. The Langmuir model presumes monolayer surface absorption with little interaction between neighbouring molecules and that all adsorption sites have the same energy. The linear version of the Langmuir model is as follows (Eq. 3):

$$\frac{C_e}{q_e} = \frac{C_e}{q_m} + \frac{1}{(K_l * q_m)} \quad (3)$$

The equilibrium cadmium ion concentration ( $C_e$ , in ppm), the quantity of  $\text{Cd}^{2+}$  adsorbed per unit mass of polymers ( $q_e$ ,  $\text{mg g}^{-1}$ ), the adsorption capacity ( $q_m$ ,  $\text{mg g}^{-1}$ ), and the adsorption equilibrium constant ( $K_l$ ,  $\text{L mg}^{-1}$ ). Non-ideal sorption on heterogeneous surfaces is assumed in the Freundlich model, which may be stated in this way (4):

$$\ln q_e = \ln K_f + \frac{\ln C_e}{n} \quad (4)$$

$K_f$  represents the Freundlich constants, and  $n$  represents the Freundlich adsorption strength exponent linked to heterogeneity. Linear regression utilizing the proper linear plot for each isotherm model is widely used to extract the values of the model parameters ( $q_{\max}$ ,  $K_l$ ,  $K_f$  and  $n$ ).

Linear plots of the Langmuir model and the Freundlich model for each polymer's adsorption by metal ions are displayed in Fig. 8a, b, respectively. The model parameters' regression values are shown in Table 3. The Freundlich model best describes the adsorption of  $\text{Cd}^{2+}$  to  $\text{PAP}_D$  in this investigation, while the Langmuir model fits better with the  $\text{PAP}_h$  data, and  $\text{PAP}_D$  was shown to have a higher sorption capacity than  $\text{PAP}_h$ .

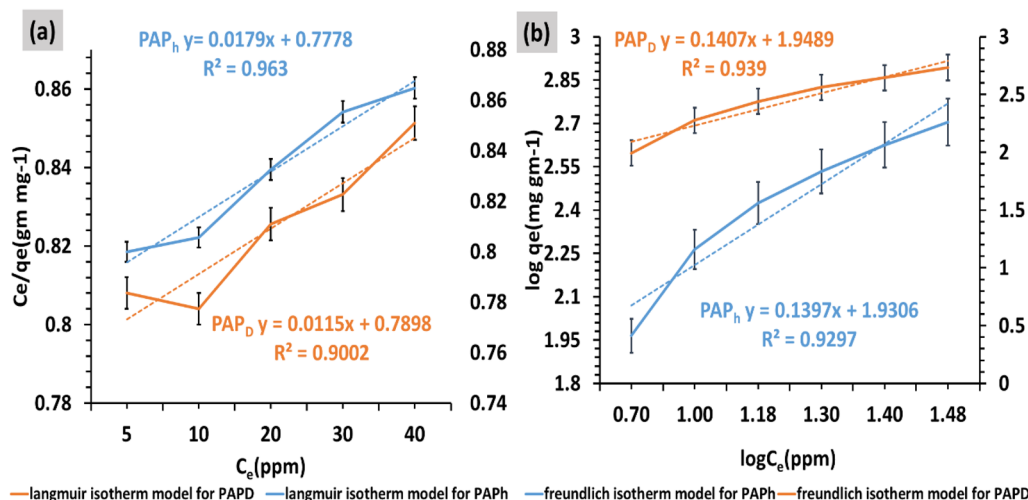


**Fig. 8** The PAP<sub>h</sub> and PAP<sub>D</sub> isotherm model for cadmium ion adsorption a Langmuir and b Freundlich

The agreement is probably because a monolayer forms on the PAP<sub>h</sub>'s surface, and intermolecular forces diminish as Cd<sup>2+</sup> ions move away from the adsorption site. Additionally, the adsorbent surface is probably more uniform than PAP<sub>D</sub> and comprised adsorption sites that have the same energy potential [68]. Larger values of *n* for PAP<sub>D</sub> than PAP<sub>h</sub> (lower values of 1/*n*) validate the high heterogeneity of the PAP<sub>D</sub> adsorbent and suggest a greater interaction between the adsorbent and the

adsorbate. Two polymers have *n* values (7.16 for PAP<sub>h</sub>, 7.11 for PAP<sub>D</sub>) that point to adsorption heterogeneity on the surface [69–71].

The adsorption capabilities of synthesized PAP<sub>h</sub> and PAP<sub>D</sub> are compared to other polypyrroles, as shown in Table 4. Compared to other polymers that have been examined, PAP polymers are superior in terms of their adsorption capability [67, 72–78].

**Table 3** Isotherm parameters for cadmium adsorption by PAP<sub>h</sub> and PAP<sub>D</sub> according to the Langmuir and Freundlich isotherm models

		Langmuir isotherm		Freundlich isotherm	
PAP <sub>h</sub>	Temperature	$K_l R^2$	$Q_m$	$K_f R^2$	<i>n</i>
	298K	0.0230 0.963 $y = 0.0179x + 0.778$	55.86	6.89 0.930 $y = 0.1397x + 1.9306$	7.16
PAP <sub>D</sub>		0.0145 0.9001 86.95		7.02 0.939 7.11	
	298K	$y = 0.0115x + 0.7898$		$y = 0.1407x + 1.9489$	

**Table 4** The prepared polymers and various fabricated AC materials compare adsorption capacity

Adsorbent material	Qe (mg g <sup>-1</sup> )	Refs.
Dithiocarbamate functionalized pyrrole-based terpolymers	14.18	[72]
Polypyrrole/graphene oxide composite	30.59	[73]
ZnO–Ag/polypyrrole	85	[74]
Polypyrrole functionalized magnetic Fe3O4 nanoparticle	19.92	[75]
Polypyrrole coated on the sawdust (PPy/SD)	28.04	[76]
Polypyrrole/Al2O3 (removal of Cd (II) by using polypyrrole and its nanocomposites	9.709	[77]
(PPy) particles obtained by oxidative polymerization of pyrrole	71.4	[78]
PAP <sub>h</sub>	55.86	Present study
PAP <sub>D</sub>	86.95	

**Adsorption kinetics**

The pseudo-first-order model (PFO), the pseudo-second-order model (PSO), the intraparticle diffusion model, and the Weber–Morris model are typical kinetic models used to describe the adsorption processes. Adsorption is a multi-step process that begins with the movement of the adsorbate from the fluid bulk to the adsorbent surface, continues with the movement of the adsorbate within the porous adsorbent (internal diffusion), and finally, involves physical or chemical binding of the adsorbate to the adsorbent surface. Accordingly, the first three models postulate that the binding rate controls the total adsorption process rate, while the final two postulate that the mass transport rate controls the total process rate. One of these two assumptions has to be adopted, or more complex models that include the adsorption process are needed in some way. Alternatively, one could use one of these two assumptions. In the case of external diffusion, factors such as surface area, surface reactivity, and liquid layer thickness had a role; in the case of internal diffusion, factors such as surface reaction and pore shape impacted both diffusion and adsorption on the activated site [75]. A specific system controls film diffusion when there is poor mixing, low concentration, small adsorbent particle sizes, and a high affinity for the adsorbate. Intraparticle diffusion is used to control when there is good mixing, large adsorbent particle sizes, high adsorbate concentration, and a low affinity for the adsorbate [76, 77]. Determining and describing the mechanisms involved in metal adsorption processes and the key factors influencing adsorption kinetics will help expand our knowledge of the adsorption process. The PFO and PSO models are popular kinetic models many researchers use. The Lagergren PFO is valid during the initial phase of an adsorption process, in which the adsorption occurs by diffusion over the contact, and the kinetics often follow the PFO rate equation. Based on Lagergren’s PFO equation, it is recognized by the adsorption Eq. (5) [78]:

$$\frac{dq_t}{dt} = K_1(q_e - q_t). \tag{5}$$

The following linear equation is obtained when this kinetic expression is integrated with the starting condition  $q_t$ :

$$\log(q_e - q_t) = \log(q_e) - \frac{K_1}{2.303}t, \tag{6}$$

where  $q_e$  and  $q_t$  are the quantities of the amount adsorbed at equilibrium ( $e$ ) and time  $t$  ( $\text{mg g}^{-1}$ ), and  $k_1$  is the equilibrium rate constant in the PFO model ( $\text{L min}^{-1}$ ). The linear graphs of  $\log(q_e - q_t)$  with time ( $t$ ) provide the value of  $k_1$ .

The PSO provides predictions throughout the adsorption isotherm by assuming that chemical sorption or chemisorption is the rate-limiting phase. The adsorption rate under these circumstances is independent of adsorbate concentration and is proportional to adsorbent capacity. The following expression represents the PSO Eq. (7):

$$\frac{t}{q_t} = \frac{1}{K_2q_e^2} + \frac{t}{q_e}. \tag{7}$$

The PSO model’s equilibrium rate constant is denoted by  $k_2$  ( $\text{g mg}^{-1} \text{min}^{-1}$ ). Table 5 approximates the parameters of the above-mentioned kinetic models based on the slope and intercept values. The  $R^2$  values of the PFO kinetic model (0.996 for  $\text{PAP}_h$ , and 0.988 for  $\text{PAP}_D$ ) are greater than that of the PSO kinetic model (0.755 for  $\text{PAP}_h$ , and 0.756 for  $\text{PAP}_D$ ), suggesting that the former provides a more accurate description of the reaction. The theoretical values of  $q_e$  ( $\text{PAP}_h$  645.06 and  $\text{PAP}_D$  663.05  $\text{mg g}^{-1}$ ) by the PFO kinetic model are closer to this experimental value of 600  $\text{mg g}^{-1}$  than the PSO kinetic model (47.85 for  $\text{PAP}_h$  and 50 for  $\text{PAP}_D$   $\text{mg g}^{-1}$ ), suggesting that the adsorption occurs primarily through diffusion across the interface. Adsorption at the solid–liquid interface involves transporting adsorbent to the material’s perimeter and molecule diffusion via the liquid layer surrounding the absorbing particles. Adsorbed molecules diffuse into the adsorbent’s

**Table 5** Kinetic parameters for the adsorption of  $\text{Cd}^{2+}$  ions adsorption using  $\text{PAP}_h$  and  $\text{PAP}_D$

	Pseudo-first-order (PFO)		Pseudo-second-order (PSO)	
$\text{PAP}_h$	$q_{e(\text{cal})} \ q_{e(\text{exp})} \ \text{mg g}^{-1} \ \text{mg g}^{-1}$ 600 645.06 $y = -0.0978x + 2.8096$ $R^2 = 0.996$	$K_1 \ \text{L min}^{-1}$ 0.225	$q_{e(\text{cal})} \ q_{e(\text{exp})} \ \text{mg g}^{-1} \ \text{mg g}^{-1}$ 600 47.85 $y = 0.0209x + 0.0162$ $R^2 = 0.755$	$K_2 \ \text{min}^{-1}$ 0.027
$\text{PAP}_D$	600 663.28 0.251 $y = -0.109x + 2.8217$ $R^2 = 0.988$		600 50.00 0.026 $y = 0.02x + 0.0154$ $R^2 = 0.756$	

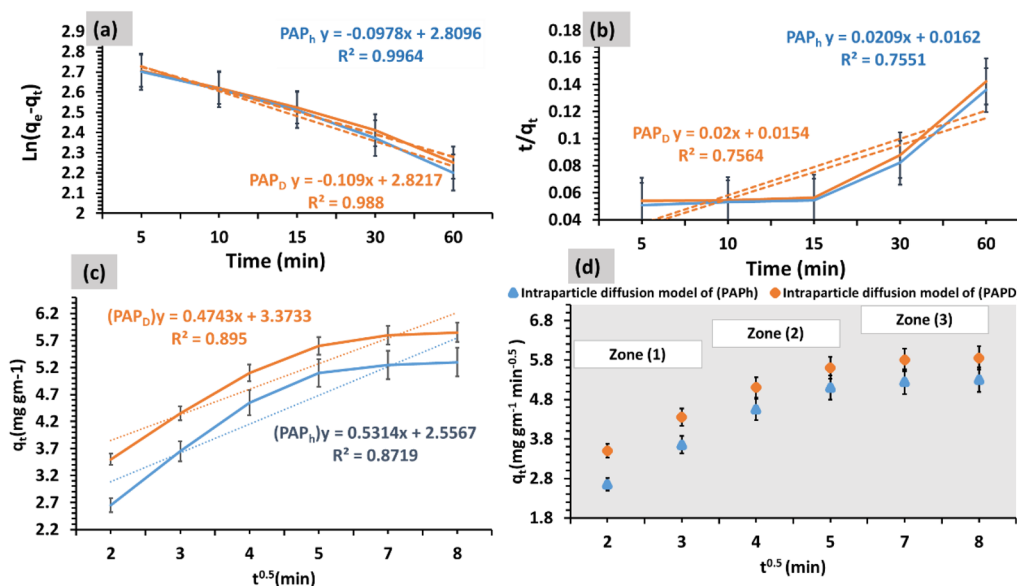


**Fig. 9** a Pseudo-first-order (PFO), b pseudo-second-order (PSO), and c, d Weber and Morris intraparticle diffusion model for Cd<sup>2+</sup> adsorption using PAP<sub>h</sub> and PAP<sub>D</sub> as adsorbents

intraparticle gaps and pores and then fix on its sites. Thus, one or both stages may control the whole procedure [79–82]. PFO assumes that sorption only occurs on localized sites, that the degree of occupation of locations for sorption is proportional to the total number of empty locations, and that sorbed ions do not interact, resulting in a single layer of adsorbates on the outside of the adsorbent. PSO model depicts the fast adsorption of divalent metal ions onto solid samples, resulting in inconsistencies between experimental and calculated results. We found that the PSO model’s linearization includes inappropriate data due to the inability to capture kinetics and the initial adsorption period.

Weber and Morris proposed the intraparticle diffusion model, which considers pore diffusion. It is the most used intraparticle diffusion equation for sorption systems. By plotting characteristic curves, one can obtain different initial adsorption factors ( $R_i$ ), and then three zones of sorption can be determined, with  $R_i$  values ranging from 1 to 0. They identified three distinct stages of adsorption: (i) powerful, (ii) intermediate, and (iii) poor [83, 84]. The formula for the diffusion of intraparticle is as follows:

$$q_t = K_i t^{0.5} + C. \tag{8}$$

The intercept C is found by extending the straight line portion of the plot of  $q_t$  against  $t^{0.5}$ , and  $k_i$  represents the intraparticle diffusion rate constant ( $\text{mg g}^{-1} \text{min}^{-0.5}$ ).

Figure 9c shows the relationship between adsorbate uptake and the square root of time ( $t^{0.5}$ ), which was determined using Eq. (8). Table 6 contains the values of the parameters that were calculated. Different theoretical frameworks provide different explanations for the

**Table 6** Diffusion parameters for the Weber and Morris intraparticle model of Cd<sup>2+</sup> ions adsorption using PAP<sub>h</sub> and PAP<sub>D</sub>

	PAP <sub>h</sub>	PAP <sub>D</sub>
Equation	$y = 0.5314x + 2.5567$	$y = 0.4743x + 3.3733$
$R^2$	0.8719	0.895
$K_i$	0.5314	0.4743
$C/q_{ref}$	0.828	0.8767
$R_i$	0.172	0.1233

intraparticle diffusion equation. A thicker boundary layer is represented by a bigger value of the arbitrary constant C, which denotes barrier layer thickness. Without boundary layers, when  $C = 0$ , the linear line should pass the origin [85]. Hence, intraparticle diffusion would continue to be the rate-controlling step during the whole adsorption kinetic process, and film diffusion could be disregarded because of no or significantly reduced thickness. According to several studies, the rate-limiting stage in most adsorption processes comprises intraparticle and film diffusion, as shown by the nonzero intercepts [86]. Additional research has shown intraparticle diffusion follows a three-step regression model with a horizontal line representing equilibrium in the macro, meso, and micropores. Researchers found three distinct linear phases in a different investigation: fast surface loading, pore diffusion, and horizontal equilibrium.

The intraparticle diffusion plots reveal a multi-linear sorption mechanism in this investigation, suggesting the presence of three functional stages (Fig. 9d). Diffusion of

sorbate molecules over the boundary layer or from the solution to the sorbent's exterior surface (PAP<sub>h</sub>, PAP<sub>D</sub>) is responsible for the first, more distinct stage. While intraparticle diffusion is the rate-limiting mechanism in the second stage of the progressive sorption process, it begins to slow down in the third stage, which is linked to the ultimate equilibrium when sorbate concentration in the solution is exceedingly low [83].

The following equations are used to calculate the initial sorption behavior as follow [87]:

$$q_{ref} = K_{iref}^{0.5} + C, \quad (9)$$

$$R_i = \left( \frac{K_i t_{ref}^{0.5}}{q_{ref}} \right). \quad (10)$$

Regarding the intraparticle diffusion model, the characteristics curve  $R_i$  may be obtained using the following equation []:

$$R_i = 1 - \left( \frac{C}{q_{ref}} \right). \quad (11)$$

Concerning the initial fast adsorption associated with film diffusion, it was noted that PAP<sub>D</sub> had a lower  $K_i$  value than PAP<sub>h</sub>, suggesting a lower surface adsorption reaction with an active site, creating an electrostatic interaction between Cd<sup>2+</sup> and PAP<sub>h</sub>'s adsorption sites. Following the same pattern as the PSO model, the PAP<sub>h</sub> rapidly achieved equilibrium, whereas the PAP<sub>D</sub> took longer. An early sorption process of significant strength was seen where  $0.5 > R_i > 0.1$  and  $0.5 < C/q_{ref} < 0.9$ , as indicated in analogous prior research [84].

#### Adsorption mechanism between polymers and Cd<sup>2+</sup> metal ion

Mechanisms for Cd<sup>2+</sup> adsorption on the synthesized polymers include surface complexation and Cd- $\pi$  interaction. FT-IR spectra after Cd<sup>2+</sup> adsorption were collected to identify the key functional groups of polymers responsible for the adsorption (Fig. 10 and Table 7). After adsorption, the peaks associated with some functional groups, those which contain oxygen C=O or nitrogen atoms C-N and C=C, either diminished or shifted to another wavenumber, suggesting that these groups play a role in the binding of Cd<sup>2+</sup> ion through complexation. An additional mechanism for metal sorption by polymers was  $\pi$ -cation interaction. Since PAP<sub>D</sub> contains more aromatic rings than PAP<sub>h</sub>, It is evident that the cyclic aromatic system may function as the  $\pi$ -donor and that the electron-donating increased stronger with the increasing number of aromatic connected rings [88, 89]. Figure 10 shows the XRD analysis of the polymers with Cd ions

adsorbed on them. Indicating that metal adsorption on the polymers' surface caused a new crystal peak to form at  $2\theta = 40^\circ$  [90].

#### Recycling performance of functionalized pyrrole-based polymer

One popular and easy way to test an adsorbent's recycling ability in heavy metal ion removal is to use the desorbing solution technique [91, 92]. Sodium hydroxide (NaOH), sodium, and hydrochloric acid (HCl) are the typical desorbing agents used in this recycling process. Sodium hydroxide and hydrochloric acid in water are powerful complexing agents for metal ion desorption and have shown promising regeneration outcomes; nevertheless, their high cost makes them unattractive for use in recycling. Aqueous solutions of them are considered to be the most cost-effective and efficient desorbents for use in recycling processes. The polymer's adsorption properties were examined across four cycles of desorption testing utilizing 0.1M concentrations of sodium hydroxide (NaOH), sodium, and hydrochloric acid (HCl) to renew the adsorbent that was used. The results are shown in Fig. 10f. Cd<sup>2+</sup> adsorption capacities decreased fast across the board as the regeneration cycles increased; PAP<sub>D</sub> was more efficient than PAP<sub>h</sub> in this regard. The adsorbent's poor adsorption capability after regeneration is due to its inefficient regeneration sites. The adsorption efficiency for Cd<sup>2+</sup> decreased after four reuse cycles, going from 94 to 84% for PAP<sub>D</sub> and 92% to 82% for PAP<sub>h</sub>; adsorption and desorption also did not change the adsorbent's mass much. Thus, polymers are reusable and possess a high adsorption capability for removing metal ions.

#### Conclusion

The Paal-Knorr reaction of PAK with hexylamine and 1,4- phenylene diamine resulted in the effective preparation of two novel polymers (PAP<sub>h</sub> and PAP<sub>D</sub>). Several analytical techniques validated structure completion, such as FT-IR spectroscopy, XRD, UV spectroscopy, and thermogravimetric (TGA) investigations, proved that PAP polymers could withstand high temperatures. SEM revealed a distinct morphology and microstructure, and according to BET's specifications, the crosslinking reaction boosted PAP<sub>D</sub>'s specific surface area. Adsorption studies revealed that PAP<sub>h</sub> had a maximum adsorption capacity for Cd<sup>2+</sup> of 55.86 mg g<sup>-1</sup>, and PAP<sub>D</sub> had a capacity of 86.95 mg g<sup>-1</sup>, indicating that the crosslinking ability effectively increased the PAP<sub>D</sub>'s adsorption capacity. It was discovered that increasing both the contact duration and the pH of the solution increased the amount of Cd<sup>2+</sup> ions adsorbed. The number of Cd<sup>2+</sup> ions adsorbed rises as the dosage of PAP polymers increases, and the adsorbent's chemical structure is related to the adsorbent's

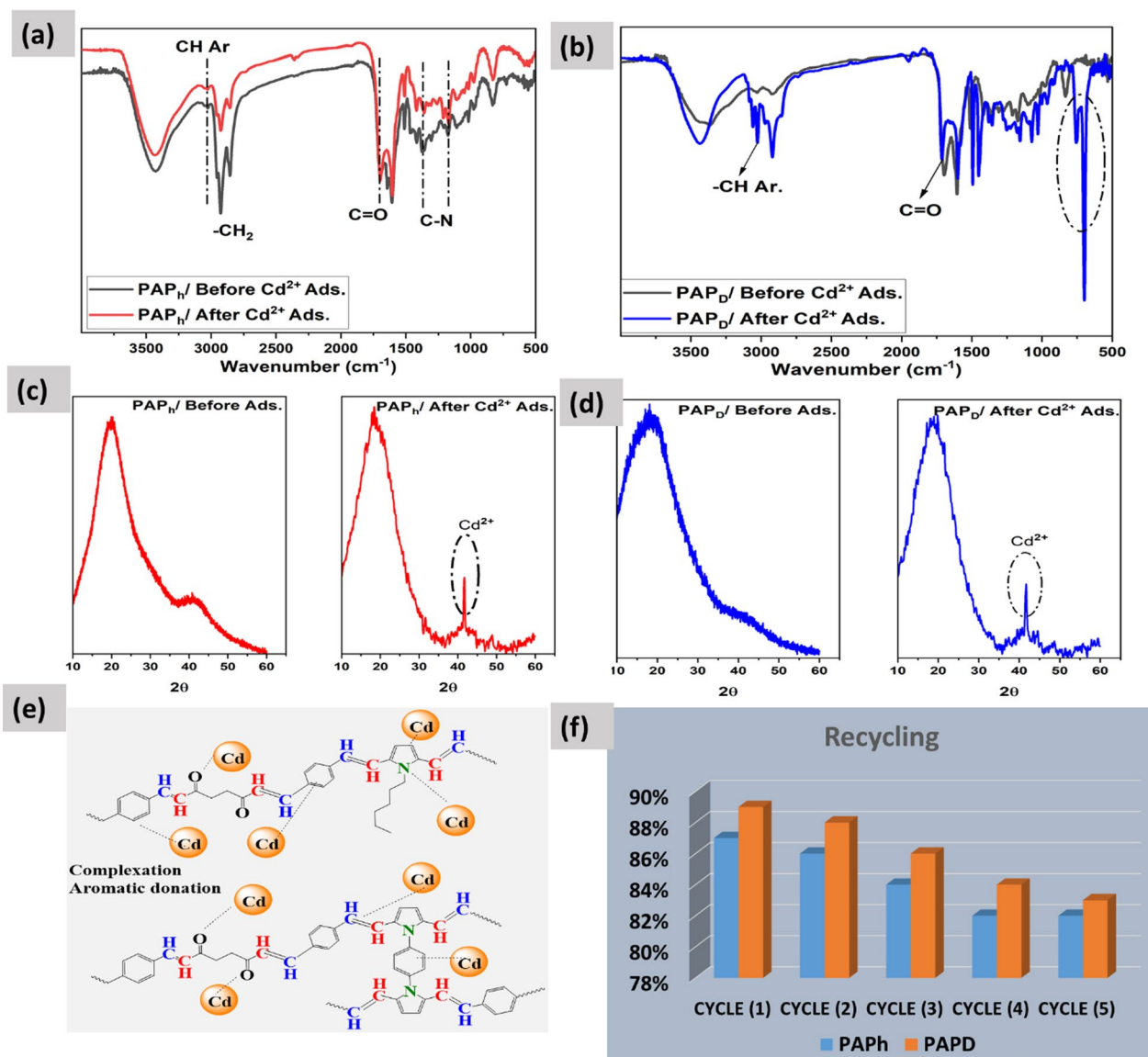


**Fig. 10** a, b Represent FT-IR. c and d are XRD before and after adsorption of Cd<sup>2+</sup> metal. e Depiction of adsorption mechanism in polymers. f Regeneration cycle of PAP<sub>h</sub> and PAP<sub>D</sub>

**Table 7** Comparison of the FT-IR spectrum properties of PAP<sub>h</sub> and PAP<sub>D</sub> before and after adsorption of Cd<sup>2+</sup> ions

IR peaks	PAP <sub>h</sub>		PAP <sub>D</sub>	
	Before Ads	After Ads	Before Ads	After Ads
C=O	1691 cm <sup>-1</sup>	1693 cm <sup>-1</sup>	1699 cm <sup>-1</sup>	1713 cm <sup>-1</sup>
C=C Py	1510 cm <sup>-1</sup>	1508 cm <sup>-1</sup>	1511 cm <sup>-1</sup>	1492 cm <sup>-1</sup>
C=C Ar	1610 cm <sup>-1</sup>	1602 cm <sup>-1</sup>	1607 cm <sup>-1</sup>	1601 cm <sup>-1</sup>
C-N	1172 cm <sup>-1</sup>	1165 cm <sup>-1</sup>	1167 cm <sup>-1</sup>	1156 cm <sup>-1</sup>
	1379 cm <sup>-1</sup>	1361 cm <sup>-1</sup>	1365 cm <sup>-1</sup>	1356 cm <sup>-1</sup>

capacity and adsorption rate. Results from the experiments' pseudo-second-order kinetic (PSO) and Freundlich isotherm models match the data well for both materials. The above findings suggested that the produced polymers PAP may be useful adsorbents in Cd<sup>2+</sup> adsorption from wastewater.

**Acknowledgments**

This work was supported by the Science, Technology & Innovation Funding Authority (STDF) in Egypt as part of the research Project (Project ID: 46993).

### Author contributions

M.S.: Conceptualization, Investigation, Resources, Writing - Review & Editing, Supervision. I.A.: Conceptualization, Methodology, Investigation, Visualization, and Writing - Original Draft. H.E.: Investigation, Resources, Writing - Review & Editing, Supervision, Project administration, and Funding acquisition. M.F.: Writing - Review & Editing, Supervision. K.A.: Resources, Writing - Review & Editing, Supervision, Project administration, and Funding acquisition.

### Funding

Open access funding provided by The Science, Technology & Innovation Funding Authority (STDF) in cooperation with The Egyptian Knowledge Bank (EKB).

### Availability of data and materials

All data generated or analysed during this study are included in this published article.

### Declarations

#### Competing interests

The authors declare no competing interests.

#### Author details

<sup>1</sup>Chemistry Department, Faculty of Science, New Valley University, El-Kharja 72511, Egypt. <sup>2</sup>Polymer Research Laboratory, Chemistry Department, Faculty of Science, Assiut University, Asyut 71515, Egypt. <sup>3</sup>Assiut Cement Company (Cemex Egypt), 18th Assiut- Elwadi Road, Asyut, Egypt. <sup>4</sup>Chemistry Department, Faculty of Science, Assiut University, Asyut 71515, Egypt. <sup>5</sup>Nanoclusters and Photocatalysis Laboratory, Chemistry Department, Faculty of Science, Assiut University, Asyut 71515, Egypt.

Received: 18 December 2023 Accepted: 19 March 2024

Published online: 01 April 2024

### References

- Phan TD et al (2018) Assessment of the vulnerability of a coastal freshwater system to climatic and non-climatic changes: A system dynamics approach. *J Clean Prod* 183:940–955
- Salehi M (2022) Global water shortage and potable water safety; today's concern and tomorrow's crisis. *Environ Int* 158:106936
- Koedrith P et al (2013) Toxicogenomic approaches for understanding molecular mechanisms of heavy metal mutagenicity and carcinogenicity. *Int J Hyg Environ Health* 216(5):587–598
- Gu Y-G, Gao Y-P, Lin Q (2016) Contamination, bioaccessibility and human health risk of heavy metals in exposed-lawn soils from 28 urban parks in southern China's largest city. *Guangzhou Appl Geochem* 67:52–58
- Zeng X et al (2016) Children with health impairments by heavy metals in an e-waste recycling area. *Chemosphere* 148:408–415
- Dadhaniya PV et al (2009) A new cationic Poly[1-vinyl-3-ethyl imidazolium iodide], P(VEl) hydrogel for the effective removal of chromium (VI) from aqueous solution. *J Macromol Sci Part A* 46(4):447–454
- Kheriji J, Tabassi D, Hamrouni B (2015) Removal of Cd(II) ions from aqueous solution and industrial effluent using reverse osmosis and nanofiltration membranes. *Water Sci Technol* 72(7):1206–1216
- Kadirvelu K, Namasivayam C (2003) Activated carbon from coconut coirpith as metal adsorbent: adsorption of Cd(II) from aqueous solution. *Adv Environ Res* 7(2):471–478
- Jung JP et al (2018) Facilitated olefin transport through membranes consisting of partially polarized silver nanoparticles and PEMA-g-PPG graft copolymer. *J Membr Sci* 548:149–156
- Buglyó P et al (2016) Metal ion binding capability of secondary (N-methyl) versus primary (N-H) dipeptide hydroxamic acids. *Polyhedron* 110:172–181
- Zhao X et al (2010) Adsorption of Pb(II) from an aqueous solution by titanium dioxide/carbon nanotube nanocomposites: kinetics, thermodynamics, and isotherms. *J Chem Eng Data* 55(10):4428–4433
- Du W et al (2014) Catalytic oxidation and adsorption of elemental mercury over CuCl<sub>2</sub>-impregnated sorbents. *Ind Eng Chem Res* 53(2):582–591
- Murugesan A et al (2014) Kinetic studies and isotherm modeling for the removal of Ni<sup>2+</sup> and Pb<sup>2+</sup> ions by modified activated carbon using sulfuric acid. *Environ Prog Sustain Energy* 33(3):844–854
- Murugesan A et al (2021) Cobalt and nickel oxides supported activated carbon as an effective photocatalysts for the degradation methylene blue dye from aquatic environment. *Sustain Chem Pharm* 21:100406
- Wang H et al (2020) Polymer-derived heteroatom-doped porous carbon materials. *Chem Rev* 120(17):9363–9419
- Wang S et al (2013) 2-(1-{2,6-Bis[bis(4-fluorophenyl)methyl]-4-methylphenylimino}ethyl)-6-[1-(arylimino)ethyl]pyridylcobalt dichlorides: Synthesis, characterization and ethylene polymerization behavior. *J Organomet Chem* 731:78–84
- Espinosa Ferao A et al (2016) Synthesis, crystal structure and DFT calculations of bis(1,3-diazinane-2-thione-κS)dicyanido disilver(I), [[Ag(Diaz)<sub>2</sub>]{Ag(CN)<sub>2</sub>}]<sub>2</sub>. *Polyhedron* 110:299–304
- Murugesan A et al (2014) Modelling of lead(II) ion adsorption onto poly(thiourea imine) functionalized chelating resin using response surface methodology (RSM). *J Water Process Eng* 3:132–143
- Loganathan M et al (2022) Effective adsorption of crystal violet onto aromatic polyimides: Kinetics and isotherm studies. *Chemosphere* 304:135332
- Wu H et al (2022) Progress and challenges in molecularly imprinted polymers for adsorption of heavy metal ions from wastewater. *Trends Environ Anal Chem* 36:e00178
- Nastasović, A., et al. Amino-functionalized glycidyl methacrylate based macroporous copolymers as metal ion sorbents. *Reactive Funct Polymers Res Adv.* 2007: p. 79–112.
- Nastasović A et al (2022) Methacrylate-based polymeric sorbents for recovery of metals from aqueous solutions. *Materials* 12(5):814
- Xiong J et al (2022) Plant transpiration-inspired environmental energy-enhanced solar evaporator fabricated by polypyrrole decorated polyester fiber bundles for efficient water purification. *J Clean Prod* 379:134683
- Millet NB (1976) The underground relief panels of King Djoser at the step pyramid complex. *J Am Res Center Egypt* 13:160–160
- Zhou Y-C et al (2021) Imidazole-functionalized polyketone-based polyelectrolytes with efficient ionic channels and superwettability for alkaline polyelectrolyte fuel cells and multiple liquid purification. *J Mater Chem A* 9(26):14827–14840
- Nastasović, A., et al., Amino-functionalized glycidyl methacrylate based macroporous copolymers as metal ion sorbents. *Reactive and functional polymers research advances*, 2007: p. 79–112.
- Nastasović A et al (2022) Methacrylate-based polymeric sorbents for recovery of metals from aqueous solutions. *Metals* 12(5):814
- Suručić L et al (2023) Speciation of hexavalent chromium in aqueous solutions using a magnetic silica-coated amino-modified glycidyl methacrylate polymer nanocomposite. *Materials* 16(6):2233
- Hamarneh AI et al (2010) Extraction of *Jatropha curcas* proteins and application in polyketone-based wood adhesives. *Int J Adhes Adhes* 30(7):615–625
- Araya-Hermosilla E et al (2022) Rapid self-healing in IR-responsive plasmonic indium tin oxide/polyketone nanocomposites. *J Mater Chem A* 10(24):12957–12967
- Orozco F et al (2020) Diels-alder-based thermo-reversibly crosslinked polymers: Interplay of crosslinking density, network mobility, kinetics and stereoisomerism. *Eur Polymer J* 135:109882
- Lima MR, G., et al (2019) Electrically self-healing thermoset MWCNTs Composites based on diels-alder and hydrogen bonds. *Polymers* 11(11):1885
- Rivas BL, Pereira ED, Moreno-Villoslada I (2003) Water-soluble polymer-metal ion interactions. *Prog Polym Sci* 28(2):173–208
- Sayed MM et al (2022) Synthesis, characterization and application of high adsorption performance of novel 1, 4-polyketone. *Sci Rep* 12(1):16317
- Mokhter M et al (2017) Preparation of polyelectrolyte-modified membranes for heavy metal ions removal. *Environ Technol* 38(19):2476–2485
- Jiang Z, Sanganería S, Sen A (1994) Polymers incorporating backbone thiophene, furan, and alcohol functionalities formed through chemical



- modifications of alternating olefin–carbon monoxide copolymers. *J Polym Sci, Part A: Polym Chem* 32(5):841–847
37. Zhang Y et al (2008) Polymeric amines by chemical modifications of alternating aliphatic polyketones. *J Appl Polym Sci* 107(1):262–271
  38. Zhang Y et al (2008) Cross-linking of multiwalled carbon nanotubes with polymeric amines. *Macromolecules* 41(16):6141–6146
  39. Vetter CA et al (2011) Novel synthesis of stable polypyrrole nanospheres using ozone. *Langmuir* 27(22):13719–13728
  40. Li X-G et al (2010) Efficient and scalable synthesis of pure polypyrrole nanoparticles applicable for advanced nanocomposites and carbon nanoparticles. *J Phys Chem C* 114(45):19244–19255
  41. Scienza LC, Thompson GE (2001) Preparation and surface analysis of PPy/SDBS films on aluminum substrates. *Polimeros* 11:142–148
  42. Li X-G et al (2009) Efficient synthesis of intrinsically conducting polypyrrole nanoparticles containing hydroxy sulfoaniline as key self-stabilized units. *The J Phys Chem C* 113(52):21586–21595
  43. Hazarika J, Kumar A (2013) Controllable synthesis and characterization of polypyrrole nanoparticles in sodium dodecylsulphate (SDS) micellar solutions. *Synth Met* 175:155–162
  44. Zhong W et al (2006) High-yield synthesis of superhydrophilic polypyrrole nanowire networks. *Macromolecules* 39(9):3224–3230
  45. Shaaban IA et al (2022) Keto–enol tautomerism, spectral (infrared, Raman and NMR) studies and normal coordinate analysis of 4-methyl-2-hydroxyquinoline using quantum mechanical calculations. *J Mol Struct* 1252:132137
  46. Cho, H., et al., *The Paal–Knorr reaction revisited. A catalyst and solvent-free synthesis of underivatized and N-substituted pyrroles*. *Green Chemistry*, 2015. **17**(2): p. 1088–1099.
  47. Krishnaswamy S et al (2022) Enhanced UV emissions in Polypyrrole/PVA composite for smart apparels. *Optik* 266:169596
  48. Yang C, Liu P (2010) Polypyrrole/conductive mica composites: preparation, characterization, and application in supercapacitor. *Synth Met* 160(7–8):768–773
  49. Bai L et al (2018) Effect of temperature, crystallinity and molecular chain orientation on the thermal conductivity of polymers: a case study of PLLA. *J Mater Sci* 53(14):10543–10553
  50. Maruthamuthu S et al (2017) Conductivity and dielectric analysis of nanocolloidal polypyrrole particles functionalized with higher weight percentage of poly(styrene sulfonate) using the dispersion polymerization method. *J Polym Eng* 37(5):481–492
  51. Yin J et al (2020) Self-assembled functional components-doped conductive polypyrrole composite hydrogels with enhanced electrochemical performances. *RSC Adv* 10(18):10546–10551
  52. Amin PO et al (2021) Synthesis, spectroscopic, electrochemical and photophysical properties of high band gap polymers for potential applications in semi-transparent solar cells. *BMC Chem* 15(1):25
  53. Galář P et al (2013) Chemical changes and photoluminescence properties of UV modified polypyrrole. *Int J Electrochem Sci* 8(1):57–70
  54. Abinaya M et al (2019) In situ synthesis, characterization, and catalytic performance of polypyrrole polymer-incorporated Ag<sub>2</sub>MoO<sub>4</sub> nanocomposite for detection and degradation of environmental pollutants and pharmaceutical drugs. *ACS Appl Mater Interf* 11(41):38321–38335
  55. Shi J, Tang CW (2002) Anthracene derivatives for stable blue-emitting organic electroluminescence devices. *Appl Phys Lett* 80(17):3201–3203
  56. Wang S et al (2018) Efficient deep-blue electrofluorescence with an external quantum efficiency beyond 10. *IScience* 9:532–541
  57. Sun M et al (2023) Highly efficient deep-blue electrofluorescence with optimized excited state composition and “hot-exciton” channel. *Dyes Pigment* 210:111002
  58. Liu G et al (2020) Reduced graphene oxide/polypyrrole composite: an advanced electrode for high-performance symmetric/asymmetric supercapacitor. *Carbon Lett* 30(4):389–397
  59. Greenfield ML, Theodorou DN (1993) Geometric analysis of diffusion pathways in glassy and melt atactic polypropylene. *Macromolecules* 26(20):5461–5472
  60. Athira AR et al (2022) Surfactant intercalated polypyrrole-exfoliated graphene oxide hybrid thin film symmetric supercapacitor. *J Mater Sci* 57(12):6749–6762
  61. Wu H et al (2021) Boosting the lithium and sodium storage performance of graphene-based composite via pore engineering and surface protection. *Nanotechnology* 32(10):105402
  62. Leay L, Siperstein FR (2013) Single polymer chain surface area as a descriptor for rapid screening of microporous polymers for gas adsorption. *Adsorpt Sci Technol* 31(1):99–112
  63. Soomro SS et al (2014) The microstructure and melt properties of CO–ethylene copolymers with remarkably low CO content. *Polym Chem* 5(12):3831–3837
  64. Ostolska I, Wiśniewska M (2014) Application of the zeta potential measurements to explanation of colloidal Cr<sub>2</sub>O<sub>3</sub> stability mechanism in the presence of the ionic polyamino acids. *Colloid Polym Sci* 292(10):2453–2464
  65. Pal A, Giri A, Bandyopadhyay A (2016) Influence of hydrodynamic size and zeta potential of a novel polyelectrolyte poly(acrylic acid) grafted guar gum for adsorption of Pb(II) from acidic waste water. *J Environ Chem Eng* 4(2):1731–1742
  66. Jun B-M et al (2020) Adsorption of selected dyes on Ti<sub>3</sub>C<sub>2</sub>T<sub>x</sub> MXene and Al-based metal-organic framework. *Ceram Int* 46(3):2960–2968
  67. Adelabu IO et al (2020) Synthesis of polyamine–CNT composites for the removal of toxic cadmium metal ions from wastewater. *J Mol Liq* 297:111827
  68. Yan L et al (2015) Magnetic biochar decorated with ZnS nanocrystals for Pb (II) removal. *ACS Sustain Chem Eng* 3(1):125–132
  69. Tan P et al (2015) Adsorption of Cu<sup>2+</sup>, Cd<sup>2+</sup> and Ni<sup>2+</sup> from aqueous single metal solutions on graphene oxide membranes. *J Hazard Mater* 297:251–260
  70. Yu Z et al (2017) Preparation and characterization of poly(maleic acid)-grafted cross-linked chitosan microspheres for Cd(II) adsorption. *Carbohydr Polym* 172:28–39
  71. Anah L, Astrini N (2018) Isotherm adsorption studies of Ni(II) ion removal from aqueous solutions by modified carboxymethyl cellulose hydrogel. *IOP Conf Series Earth Environ Sci* 160(1):012017
  72. Al Hamouz OCS, Estatie M, Saleh TA (2017) Removal of cadmium ions from wastewater by dithiocarbamate functionalized pyrrole based terpolymers. *Separat Purif Technol* 177:101–109
  73. Xue J et al (2020) Preparation of a polypyrrole/graphene oxide composite electrode by electrochemical codeposition for capacitor deionization. *ACS Omega* 5(19):10995–11004
  74. Mohamed F et al (2021) Design and characterization of a novel ZnO–Ag/Polypyrrole core-shell nanocomposite for water bioremediation. *Nanomaterials* 11(7):1688
  75. Obradović B (2020) Guidelines for general adsorption kinetics modeling. *Hemijaska Industrija* 74(1):65–70
  76. Ramírez-Rodríguez T, de Landa Castillo-Alvarado F (2011) Application of the intra-particle diffusion model for activated carbon fibers in an aqueous medium. *MRS Online Proc Library* 1373(1):424
  77. An B (2020) Cu(II) and As(V) adsorption kinetic characteristic of the multi-functional amino groups in Chitosan. *Processes* 8(9):1194
  78. Sahoo TR, Prelot B (2020) 7 Adsorption processes for the removal of contaminants from wastewater the perspective role of nanomaterials and nanotechnology. In: Bonelli B et al (eds) *Nanomaterials for the detection and removal of wastewater*. Elsevier, Amsterdam
  79. Petrovic B, Gorbounov M, Masoudi Soltani S (2021) Influence of surface modification on selective CO<sub>2</sub> adsorption: a technical review on mechanisms and methods. *Microporous Mesoporous Mater* 312:110751
  80. Franco DSP et al (2021) Highly effective adsorption of synthetic phenol effluent by a novel activated carbon prepared from fruit wastes of the *Ceiba speciosa* forest species. *J Environ Chem Eng* 9(5):105927
  81. López-Luna J et al (2019) Linear and nonlinear kinetic and isotherm adsorption models for arsenic removal by manganese ferrite nanoparticles. *SN Appl Sci* 1(8):950
  82. Murugesan A et al (2014) Kinetic studies and isotherm modeling for the removal of Ni<sup>2+</sup> and Pb<sup>2+</sup> ions by modified activated carbon using sulfuric acid. *Environ Progress Sustain Energy* 33(3):844–854
  83. Ofomaja AE (2010) Intraparticle diffusion process for lead (II) biosorption onto mansonia wood sawdust. *Biores Technol* 101(15):5868–5876
  84. Ofomaja AE, Ho Y-S (2007) Effect of pH on cadmium biosorption by coconut copra meal. *J Hazard Mater* 139(2):356–362
  85. Wang W et al (2019) Adsorption behavior and mechanism of emerging perfluoro-2-propoxypropanoic acid (GenX) on activated carbons and resins. *Chem Eng J* 364:132–138
  86. Ho YS, Mckay G (1998) The kinetics of sorption of basic dyes from aqueous solution by sphagnum moss peat. *Can J Chem Eng* 76(4):822–827

87. Wu FengChin WF, Tseng RuLing TR, Juang RueyShin JR (2009) Initial behavior of intraparticle diffusion model used in the description of adsorption kinetics. *Chem Eng J*. <https://doi.org/10.1016/j.cej.2009.04.042>
88. Es-said A et al (2021) Comparative adsorption studies of cadmium ions on phosphogypsum and natural clay. *Scientific African* 13:e00960
89. Tran HN, You S-J, Chao H-P (2015) Effect of pyrolysis temperatures and times on the adsorption of cadmium onto orange peel derived biochar. *Waste Manage Res* 34(2):129–138
90. Liu L, Fan S (2018) Removal of cadmium in aqueous solution using wheat straw biochar: effect of minerals and mechanism. *Environ Sci Pollut Res* 25(9):8688–8700
91. Jiang L et al (2023) Removal of manganese from water by modified groundwater plant sludge: Mechanism and application as filter media. *J Water Process Eng* 51:103418
92. Vieira RS, Beppu MM (2006) Interaction of natural and crosslinked chitosan membranes with Hg (II) ions. *Colloids Surf A* 279(1–3):196–207

### **Publisher's Note**

Springer Nature remains neutral with regard to jurisdictional claims in published maps and institutional affiliations.